PAPER

Macroscopic Visualization of a Radiated Emission Source Using Cylindrically Scanned Electric Field Amplitude Data

Yasuhiro ISHIDA[ta)], Masato KAWABATA[t], *and* Nobuo KUWABARA[tt], *Members*

SUMMARY In order to efficiently mitigate emissions radiated from electrical equipment, emission source visualization methods need to be studied. In this paper, we propose a new macroscopic visualization method based on an optimization process which uses only cylindrically-scanned electric field amplitude data from an EMI test facility as specified by CISPR, and so does not need a special measurement system. The presented method divides the visualization space into three-dimensional rectangular cells, and estimated current values through the optimization process are sorted into each corresponding cell. By displaying the summed value of every cell, the emission source can be visualized. For this study, the spatial resolution was evaluated by computer simulation, with a result of around 0.2 m using a cell size of 0.1 m. With subsequent experimental verification using a comb generator in a semi-anechoic chamber, the visualization deviation was found to be less than 0.1 m in a frequency range of 100 MHz to 800 MHz. When two spherical dipole antennas were used, the deviation was less than 0.15 m. Finally, visualization results from a facsimile unit and a PC as real EUTs were shown and basic applicability of this method demonstrated.
key words: radiated emission, visualization, EMI, CISPR

1. Introduction

The levels and measurement methods of emissions radiated from electric and electronic equipment have been specified by CISPR (International Special Committee on Radio Interference) [1]. Generally speaking, it is very difficult and costly to mitigate emission levels. One reason for this is that emission sources of an EUT (Equipment Under Test) cannot be identified easily. The objective of our research is to propose an emission source visualization method that is effective in mitigating emissions.

One of the methods currently in use is to measure the near electromagnetic field [2]. However, the relationship to measured values in the far field has not been elucidated. Visualization methods using far field measurement data include MUSIC (Multiple Signal Classification) [3] and the Holographic Method [4], which both require phase data as well as amplitude data of the electromagnetic field. The visualization spatial resolution of the Holographic Method is a half wavelength or more. Furthermore, new methods have been proposed where SPM (Sampled Pattern Matching) was applied [5] or the MUSIC algorithm was modified [6]. The spatial resolutions of these methods are better than a half

wavelength, and they can be effective, particularly for high frequencies of around 1 GHz or more, but they require the measurement system to be specially equipped. For frequencies of less than a few ten MHz, a localization method of the electromagnetic source has been presented in which the MUSIC algorithm is applied [7].

Furthermore, a radiated emission source finding method has been proposed [8]. Its target frequency ranges from 30 MHz to 1 GHz, as is used in the CISPR standard. For this method, unknown source positions and current values are calculated through an optimization process called the Marquardt method [9]. This uses cylindrically-scanned electric field amplitude data obtained from an EMI test facility as specified by CISPR. As this facility is widely used throughout the world, it is thought that this method can be used easily and its validity for two ideal sources has been shown [8]. Consequently, in order to apply this method to actual equipment, it was necessary to give optimum calculation parameters and to avoid a local minimum problem, whereby these parameters and the method of determining the most possible source positions were presented [10]. However, the determined source positions tend to be averaged to one point due to the procedure of renumbering sources in the calculation. This problem affects the accuracy and limits the applicability.

In this paper, this method is improved and a new macroscopic visualization method is proposed. Following the description of its procedure, the spatial resolution for two sources is evaluated by a computer simulation. Then, the applicability is experimentally verified using a comb generator and two spherical dipole antennas in a semi-anechoic chamber. Finally, visualization results from actual equipment are shown and conclusions made.

2. Visualization Method

2.1 Basic Model and Optimization Process

The original EUT is substituted by an equivalent set of small dipoles such that its calculated electric field amplitude is equal to the measured one [8], [10].

Figure 1 shows the coordinate system and source model. J_n is the current vector of the n th ($= (1 \cdots N)$ th) current source, and (x_n, y_n, z_n) is its position. J_n is composed of (Jx_n, Jy_n, Jz_n), which includes a real and imaginary part. N is the total source number and these values are unknown. $P_m(x_m, y_m, z_m)(m = 1 \cdots Q)$ is the position of a cylindrically
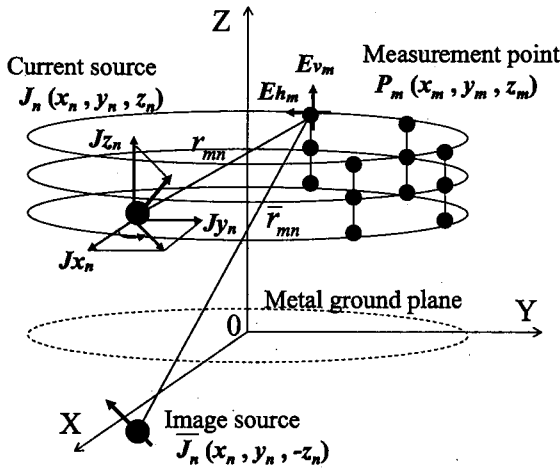
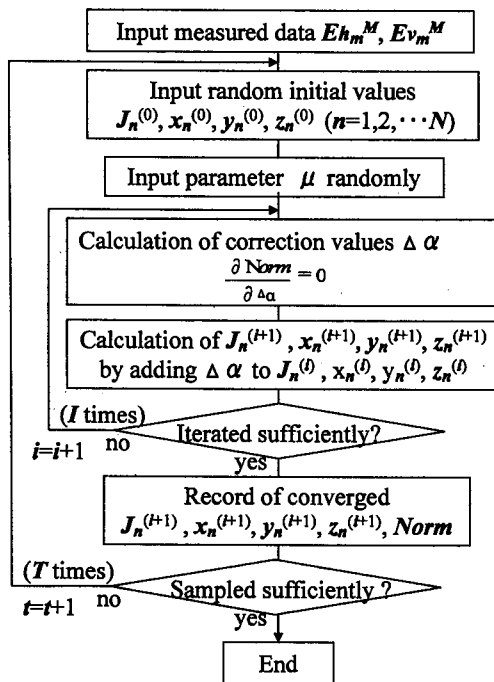**Fig. 1** Coordinate system and source model.

Fig. 2 Optimization process.

scanned measurement point which is obtained by a function of both the orientation of the EUT and a scan of the receiving antenna which is available from an EMI test facility as specified by CISPR. r_{mn} is the distance between the source position and the measurement point P_m. An upper bar indicates the image one due to the metal ground plane. Eh_m and Ev_m are the horizontal and vertical electric field amplitudes at P_m respectively.

Although only the n th source is illustrated in the figure, Eh_m and Ev_m are superposed by N sources, where it is assumed that there are N coherent sources and their radiated emissions are continuous, from which quasi-peak levels at the measurement points are stabilized.

Figure 2 shows the optimization process, in which the

Marquardt method [9] is used in order to estimate the unknown values [8], [10]. Firstly, measured electric field amplitude data is inputted, and the iteration starts with the randomly given initial values $J_n^{(0)}, (x_n^{(0)}, y_n^{(0)}, z_n^{(0)})$. The Marquardt constant μ, which strongly influences the convergence and stability of the optimization [9], is given randomly in order to expand the generality of the solutions. Correction values are calculated through (1) so as to minimize $Norm$ in the optimization. α represents unknown values.

$$\frac{\partial Norm}{\partial \Delta \alpha} = 0 \tag{1}$$

$Norm$ is the deviation between E_m^M and $E_m^{(i+1)}$ as defined in (2).

$$Norm = \frac{\sum_{m=1}^{Q} |E_m^{(i+1)} - E_m^M|^2}{\sum_{m=1}^{Q} |E_m^M|^2} \tag{2}$$

E_m^M is the horizontal or vertical electric field amplitude measured at P_m, and $E_m^{(i+1)}$ is the amplitude calculated by using the estimated values. $E_m^{(i)}$ is expressed as shown in (3) [11].

$$E_m^{(i)} = \sum_{n=1}^{N} \left\{ \frac{J_n^{(i)} e^{-jkr_{mn}}}{r_{mn}} D_{mn} + \frac{\overline{J_n^{(i)}} e^{-jk\overline{r_{mn}}}}{\overline{r_{mn}}} \overline{D_{mn}} \right\} \tag{3}$$

Where k ($=2\pi$ /wavelength) is the wave number, D_{mn} is the directivity due to the measurement antenna, and the superscript (i) shows that it is estimated by iterating i times. The coefficient is omitted because current values are normalized in this calculation. Details of this are described in Refs. [8], [10].

The calculation above is iterated I times, which is sufficient to converge the calculation, and the converged values and $Norm$ are recorded. These results depend on initial values, and may be locally minimized or diverging. Therefore, the next iteration starts with different initial values, and this trial is repeated a sufficient number, T times.

2.2 Previous Method for Estimating Source Position

For the previous method in Ref. [8], after the optimization process described in 2.1, the minimum $Norm$ case is selected from all the records (= J_n, x_n, y_n, z_n, and $Norm$). For example, assuming that ten solutions with a small $Norm$ were obtained, nine solutions might have true values and one solution might have an erred value. However, by using the method in Ref. [8], it is possible that one erred solution may become the final result due to accidental error, a locally minimized solution, measurement error, etc.

Next, Fig. 3 shows the method in Ref. [10], using the example of $N = 3$. After the optimization process described in 2.1, every recorded J_n, x_n, y_n, z_n, and $Norm$ is renumbered in order of magnitude of $|J_n|$. The first group is the set of results with the biggest $|J_n|$. The second group is that with the second largest, and the third group is that with the third
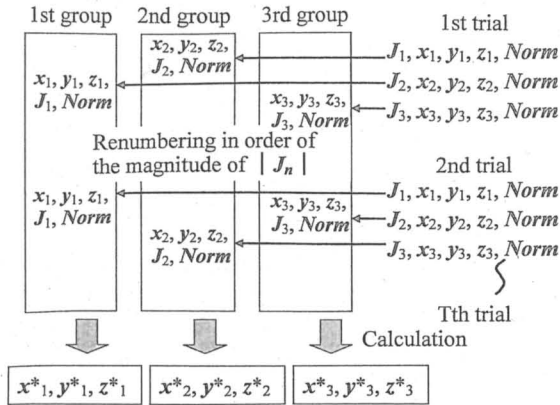
Fig. 3 Method for estimating the source position in Ref. [10].

Fig. 4 New method for macroscopic source visualization.

Fig. 5 Procedure for source visualization for the presented method.

largest. After renumbering, the best possible source position $(x_1^*, y_1^*, z_1^*), (x_2^*, y_2^*, z_2^*), (x_3^*, y_3^*, z_3^*)$ is calculated from the first group, second group and third group, respectively. w_n^* is defined in (4), where w means x, y, z, generally.

$$w_n^* = \frac{\sum_{t=1}^{T} w_n(|J_n|/Norm)}{\sum_{t=1}^{T}(|J_n|/Norm)} \qquad (4)$$

Where "divided by *Norm*" means that it is weighted according to the possibility of estimated results. This is because the smaller the *Norm*, the better the convergence. Therefore, among sufficient random trials, even if just a few cases result in a small *Norm* due to accidental error or locally minimized calculation, they negligibly influence the consequent visualization.

Using this method, however, the renumbering does not always correspond to the actual source distribution. In the case of multiple sources with even current, renumbering at each trial may be random. In this case, original sources no.1, 2, $\cdots$, N are not sorted into the first group, second group, $\cdots$, Nth group, respectively. The determined source positions tend to be averaged to one point, which is generally the center of three sources in the example case of $N = 3$.

2.3 New Method for Macroscopic Source Visualization

In this section, we propose a new method that overcomes the problem encountered in 2.2, and furthermore can be applied as a macroscopic source visualization method. For this end, the visualization space is three-dimensionally divided into rectangular cells. Figure 4 shows the example of a 0.1 m cell with $N = 3$, where the visualization space size can be given arbitrarily. Cell size is described in 3.3.

After the optimization process described in 2.1, as shown in Fig. 5, the recorded $|J_n|/Norm^2$ values are sorted into the cells in which the estimated (x_n, y_n, z_n) values are located. If its position is outside of the given visualization space, the value is excluded. Next, sorted values are summed at each cell. By displaying the value of every cell, the distribution map is obtained according to source existence possibility. Subsequently, the emission source is visualized corresponding to its distribution map.
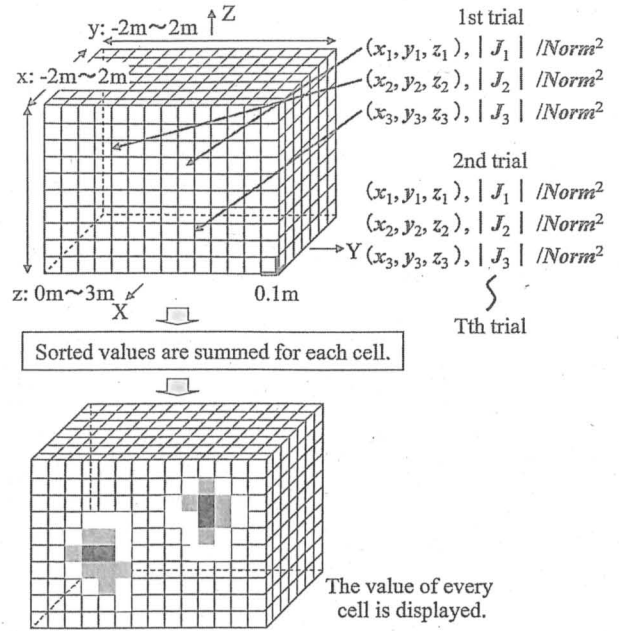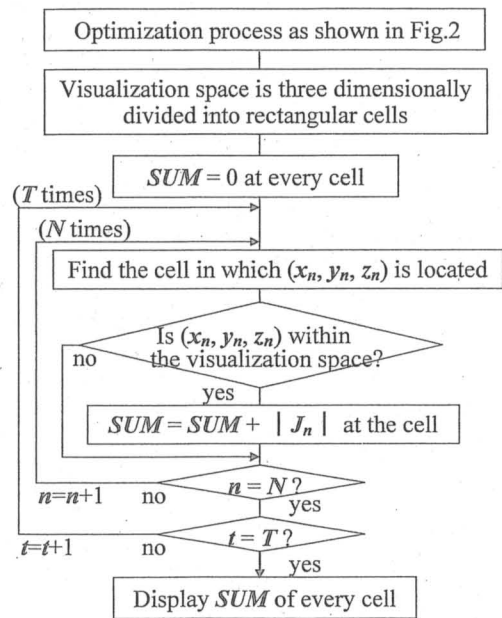
However, the result obtained in the presented optimization process is not the only theoretical solution. Therefore, as described above, the optimization is repeated as required with random initial values and the Marquardt constant μ, and the estimated results are totally used. The measurement point number Q, source number N, iteration number I, and random trial number T are given according to the previous study in order for the obtained results to be stabilized and determine the desired solution. Furthermore, unsuitable solutions are excluded by limiting the existence space. The results from the presented method indicate the "distribution

of source existence possibility," which gives effective information about the actual radiated emission reduction.

3. Evaluation by Computer Simulation

Visualization results from the presented method are discussed, where cylindrically-scanned electric field amplitude data calculated with a computer is used.

3.1 Parameters

In Ref. [10], the total source number N, the iteration number I, the random trial number T, and the parameters of the measurement points are discussed for that method. It has also been reported that these parameters can be simplified in order to shorten the calculation time for emission source modeling [12].

Since the presented method uses the same optimization process, with the help of these references, the parameters in this paper are given as shown in Table 1. N and I are given as a minimum requirement. T is given so as to be able to sample sufficiently for visualization. The measurement distance is 3 m, and the angular spacing of the measurement points is 15 degrees. The antenna height is 1 m $\cdots$ 4 m with a 0.2 m spacing (under 800 MHz) and a 0.1 m spacing (800 MHz or more).

These parameters are common for both computer simulation and experimental verification as described in Sect. 4. Experimental Verification.

3.2 Visualization Example

Firstly, we assumed two point source currents (infinitesimal dipoles) at 300 MHz, whose original current values were $(Jx_1, Jy_1, Jz_1) = (1, 0, 0.5)$ and $(Jx_2, Jy_2, Jz_2) = (0, 0.5, 0.25)$ with a phase difference of 0 degrees, namely $|J_1| : |J_2| = 1:0.5$, as an example. The original positions were $(x_1, y_1, z_1) = (0.5\,\text{m}, 0.5\,\text{m}, 1.2\,\text{m})$ and $(x_2, y_2, z_2) = (-0.2\,\text{m}, 0\,\text{m}, 1.5\,\text{m})$.

Figure 6 shows the visualization result for a 0.1 m cell. It shows the top and side view of the visualization space, in which the values are normalized, as the maximum one is 1. In the top view, each value indicates the total value of a $z = 0\,\text{m} \cdots 3\,\text{m}$ cell at each 0.1 m square $y - x$ area. In the side view, each value shows the total value of an $x = -2\,\text{m} \cdots 2\,\text{m}$ cell at each 0.1 m square $y - z$ area.

The map reveals that two sources appear at (0.5 m, 0.5 m, 1.2 m) and (−0.2 m, 0 m, 1.5 m), and these agree well with the original source positions. The normalized current amplitudes of source no.1 and 2 are 1 and 0.49, respectively; the 0.49 point is so small that it may be difficult to see in the figure. Where 5 in 120 random trials resulted in a particularly small $Norm$, almost the same converged results were obtained. For each random trial, $|J_1|/Norm^2$, $|J_2|/Norm^2$, $|J_3|/Norm^2$ retains its original current amplitude relationship, so this relationship is reproduced even if $|J_n|/Norm^2$ is summed. Thus we suppose that the visualized result can

Table 1 Calculation parameters.

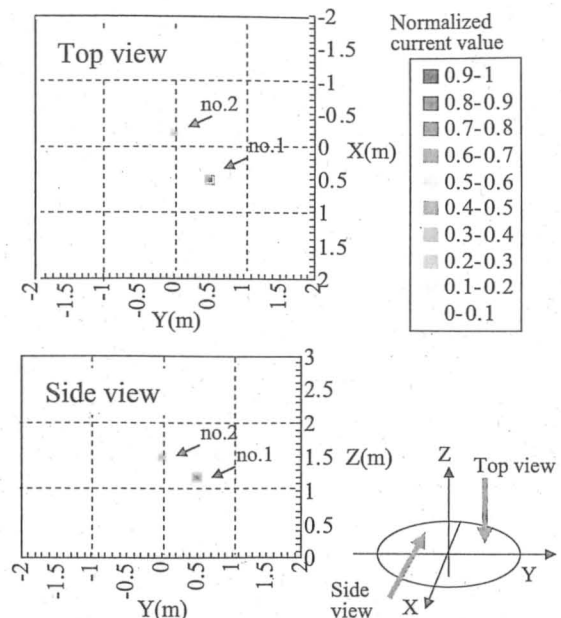| Frequency	Source number N	Iteration number I	Random trial number T
$\leq$ 300 MHz	3	150	120
$\leq$ 400 MHz	4	150	120
$\leq$ 1 GHz	5	150	120

Fig. 6 Example of a visualization result by computer simulation (cell size = 0.1 m, frequency = 300 MHz).

roughly indicate the original current amplitude relationship for simple models.

Additionally, although it is not shown in the figure, when the original current position or direction was changed, the corresponding results were obtained. The calculation time for this visualization depends on source number N and measurement points number Q, because iteration number I and random trial number T are fixed for this paper. It took around 5 minutes ($f \leq 300\,\text{MHz}$, $N = 3$, $Q = 384$), 6 minutes (300 MHz$< f \leq 400\,\text{MHz}$, $N = 4$, $Q = 384$), 9 minutes (400 MHz$< f <800\,\text{MHz}$, $N = 5$, $Q = 384$), and 15 minutes (800 MHz$\leq f \leq 1\,\text{GHz}$, $N = 5$, $Q = 768$) with a personal computer (PC/AT compatible, CPU: Pentium 4-2.8 GHz, memory: 2 GB).

3.3 Spatial Resolution for Two Sources

The spatial resolution of the presented method for two sources was investigated next. Figure 7 shows the minimum distance by which two sources can be visualized separately. For this, the current ratios $|J_1| : |J_2|$ were 1:1 and 1:0.25; (x_1, y_1, z_1) was fixed at (0 m, 0 m, 1.4 m) and (x_2, y_2, z_2) was changed to several different positions. The cell sizes were 0.1 m and 0.05 m. The results obtained by using the method in Ref. [8] are also shown.

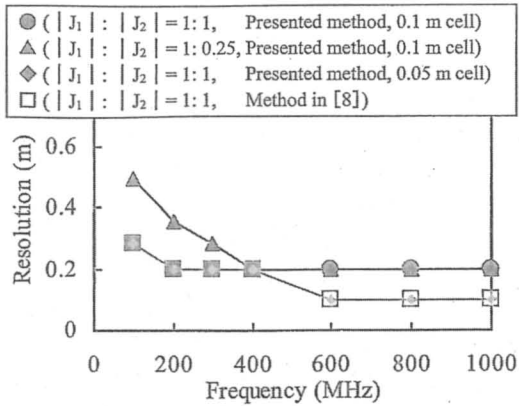Figure 7 shows that the resolution from the presented

Fig. 7 Spatial resolution for two sources.

Fig. 8 Influence of additional random noise on cylindrically scanned data.

Table 2 Deviation with a weighting of divided by $Norm, Norm^2, Norm^3$.

Frequency (MHz)	Random noise(dB)	Deviation(m)		
		$/Norm$	$/Norm^2$	$/Norm^3$
	0	0	0	0
100	±2	0.2	0.12	0.12
	±4	invisible	0.38	0.38
	0	0	0	0
800	±2	0	0	0
	±4	invisible	0.1	0.1

method with a 0.1 m cell is 0.2 m, which is equal to twice the cell size, at 200 MHz or more in the case of $|J_1| : |J_2| = 1{:}1$, and at 400 MHz or more in the case of $|J_1| : |J_2| = 1{:}0.25$. The resolution deteriorates as the frequency lowers, and the separation did not occur at less than 100 MHz. This is because the longer the wavelength, the less the radiation pattern varies. At low frequencies, the difference between the distance of a direct wave and that of a reflected wave is small compared with the wavelength. It is the same for the difference between multiple sources. In particular, the height pattern has a small null point at 100 MHz or less, which affects the source estimation accuracy. When the current ratio is unbalanced, the bigger source dominates the radiation pattern and the two sources tend to behave as one source.

Furthermore, when the cell size was 0.05 m, the resolution improved to 0.1 m at a frequency of 600 MHz or more. However, eightfold cell numbers are required. The resolution did not improve to 0.1 m at under 600 MHz; which is related to the lack of radiation pattern variation due to the wavelength. As a typical value, the cell size is given as 0.1 m in this paper. In fact, it can be decided on according to the required resolution and the allowable calculation time. The results from the method in Ref. [8] are equal to those from the presented method with a 0.05 m cell.

On the other hand, the method in Ref. [10] could not distinguish between two sources of $|J_1| : |J_2| = 1{:}1$, and so it is not shown on the figure. This is caused by misrenumbering as described in 2.2, and reveals the advantage of the presented method compared with the method in Ref. [10].

3.4 Influence of Additional Random Noise on Cylindrically Scanned Data

Here, the influence of additional random noise on cylindrically-scanned data is discussed. The given model is the same as shown in 3.2, and Fig. 8 shows the deviation between the visualized and original source positions, in which 'deviation' means the average value for source no.1 and no.2. The horizontal axis indicates the maximum level of added random noise. The results obtained by using the
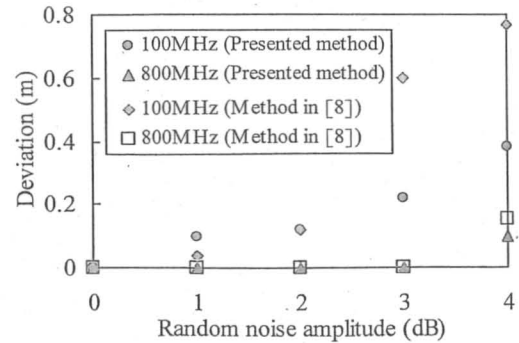
method in Ref. [8] are also shown.

It can be seen that the deviation increases by adding random noise, and that it is particularly big at the case (± 3 dB and ± 4 dB, 100 MHz, using the method in Ref. [8]). The method in Ref. [8] is easily influenced by additional noise due to the reason described in 2.2. From this point of view, the presented method is superior to the method in Ref. [8]. The deviation is small for 800 MHz; this is because the variation of the radiation pattern is such that actual information quantity remains.

For this paper, weighting is done by "divided by $Norm^2$." In order to compare it with "divided by $Norm$" or "divided by $Norm^3$," Table 2 shows the deviation using each weighting. In the case of a random noise of 0 dB, the deviation is 0 m for each weighting. As this is a relative simple source model, only a few trials among 120 result in a particularly small $Norm$. When "divided by $Norm$," for the case of ± 2 dB at 100 MHz, the deviation increases due to insufficient weighting. Moreover, in the case of ± 4 dB at 100 MHz or 800 MHz, source no.2 could not be visualized. On the other hand, the results from "divided by $Norm^3$" are equal to those from "divided by $Norm^2$," and so both can be determined. However, the value of "$Norm^4$" or "$Norm^5$" is sometimes too small to use for division. Therefore, all results are obtained from "divided by $Norm^2$" for this paper.

3.5 Influence of Error on Measurement Distance

Next, the influence of the error on cylindrically-scanned position information is discussed. The given model is the same as described in Sect. 3.2. Figure 9 shows the deviation between the visualized and original source position, in which 'deviation' means the average value for source no.1 and
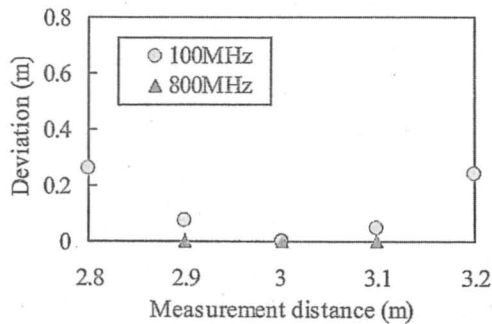
Fig. 9 Influence of error on measurement distance.

Fig. 10 Experimental system.

no.2. The horizontal axis shows the distance between the co-ordinate center and the cylindrically-scanned surface; the distance used in the optimization process was 3 m.

It can be seen that the deviation is under 0.1 m with a distance error of 0.1 m. With a distance error of 0.2 m at 800 MHz, source no.2 could not be visualized, so it is not marked in the figure. This is caused by the fact that the distance error of 0.2 m is not negligible compared with the wavelength at 800 MHz (= 0.375 m).

4. Experimental Verification

The effectiveness of the presented method was evaluated by experimental verification in a semi-anechoic chamber. The parameters are the same as given in Sect. 3.1.

4.1 Experimental System

The experimental system is shown in Fig. 10. The floor is a metal ground plane. Radiated emission from an EUT was measured using a BiConiLog antenna located 3 m from the turntable center, and its quasi-peak level was measured with an EMI receiver. For the calculation, the measurement distance is given according to the phase center of the receiving antenna at each frequency. In the horizontal electric field calculation, E plane directivity of the receiving antenna is used for the horizontal plane and non-directivity is used for the vertical plane. For the vertical electric field calculation, E plane directivity of the receiving antenna is used for the vertical plane and non- directivity is used for the horizontal plane. By rotating the turntable and scanning the measurement antenna height, the measurement points are distributed cylindrically. The complete measurement for both horizontal and vertical polarization at one frequency took around 20 minutes.

4.2 Results with a Comb Generator

A comb generator was used as an EUT; this consists of a monopole antenna, a signal generator, and an internal battery. This was determined as Model 1, Model 2, and Model 3 as shown in Table 3. Figure 11 shows an overview of the experiment.
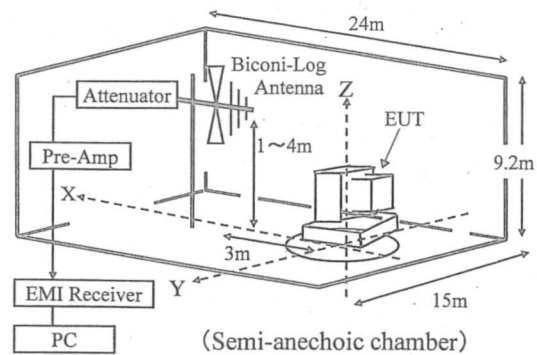
As for the results, Fig. 12 shows the deviation between

Table 3 Given models for verification.

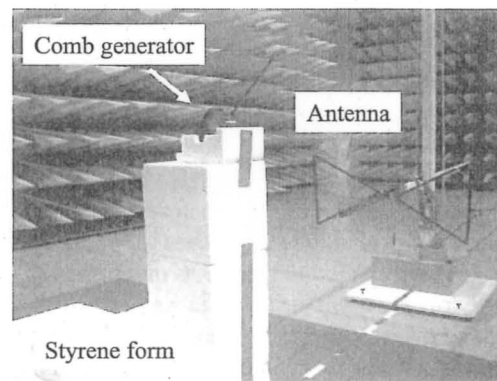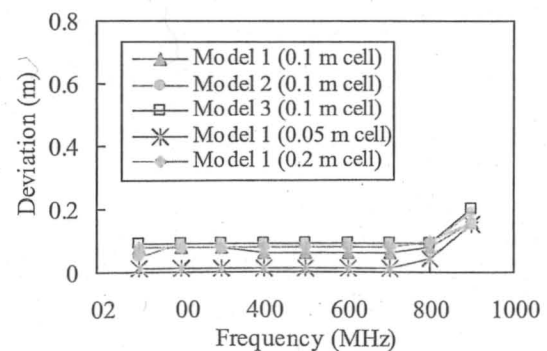| Frequency	Current ratio $\|Jx_1\| : \|Jy_1\| : \|Jz_1\|$	Source position (x_1, y_1, z_1) m
Model 1	1:0:0	(0.4, −0.45, 1.14)
Model 2	0:1:1	(0.4, −0.45, 1.22)
Model 3	0:1:1	(0.6, −0.65, 1.54)

Fig. 11 Overview of experiment.

Fig. 12 Deviation between visualized and original source position for a comb generator.

the visualized and original source position. Results for Model 1 with a cell size of 0.05 m and 0.2 m are also shown. Since it can be seen that the deviation is less than 0.1 m at a frequency range of 100 MHz to 800 MHz for each model, the basic applicability to one ideal source has been experimentally verified. Particularly, the case of a 0.05 m cell

demonstrates good accuracy. The results using a 0.2 m cell are almost the same as those with 0.1 m; this is caused by the fact that the minimum distance between the cell center and the given source position is almost equal. It is assumed that the deviation mainly depends on the cell size, and some error factors from the measurement.

The deviation is around 0.2 m at 900 MHz, one reason for which is that the radiation level from the comb generator falls and the S/N ratio decreases at high frequencies. It is also necessary to study the data quantity (= number of measurement points), calculation parameters (= source number N, iteration number I, random trial number T), and the cell size at high frequencies. For this paper, therefore, a range of 100 MHz to 800 MHz is regarded as an ideal applicable frequency range; it is planned to expand its applicability to frequencies above 800 MHz in the future.

4.3 Results with Two Spherical Dipole Antennas

The applicability to an EUT with two sources was verified. As shown in Fig. 13, two electric signals with locked phase are individually converted into optical signals by electrical-to-optical (E/O) converters. Two spherical dipole antennas (SDA) convert the optical signals into the radiated electromagnetic waves. An SDA is an antenna whose radiation properties agree well with those of a small dipole current, and the driving signal lines hardly affect the electric field because optical fibers are used. The given model used was the same as shown in Sect. 3.2.

As for the results, Fig. 14 shows the deviation between the visualized and original source positions by using the presented method and the method in Ref. [8], in which the deviation means the average value for source no.1 and no.2. It can be seen that the deviation seen by using the presented method is less than 0.15 m in a frequency range of 100 MHz to 800 MHz, and in particular, results in good accuracy at above 200 MHz. It is generally superior to the deviation by the method described in Ref. [8], although the discrepancy is not significant because the error factor in this measurement
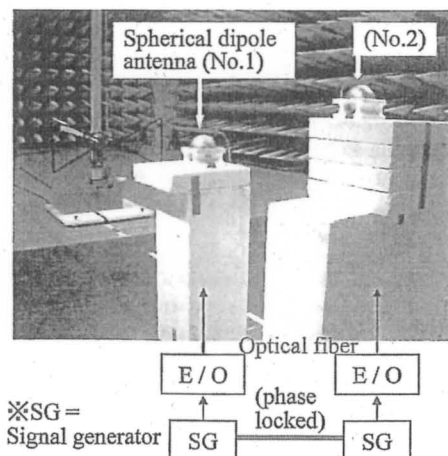
environment was relatively small. The result at 900 MHz was not marked in the figure because source no.2 was invisible; this problem does not occur when $|J_2|$ is comparable to $|J_1|$. These were common factors for both methods. More detail and the applicability to frequencies above 800 MHz, as described in Sect. 4.2, need to be studied in the future.

4.4 Results with a Facsimile Unit as an Actual EUT

A facsimile unit was used as an actual EUT. Figure 15 shows the overview of this experiment. The system consisted of a facsimile main unit placed on a 0.8 m high nonmetallic table, and a power cable. In order to pick up noticeable frequencies, pre-measurement was performed with a spectrum analyzer that records the peak-hold of the radiated emission. For the focused frequency, 240 MHz was chosen. When the main unit was shielded using a conductive sheet, the radiation level was reduced by around 20 dB. When the placement of the power cable was changed or some ferrite cores added, the radiation level changed negligibly. Therefore, it could be supposed that the dominant source exists on the main unit.

The visualization result obtained by using the presented method is shown in Fig. 16, where three sources were used as shown in Table 1. It can be seen that sources are visualized on the rear part of the main unit, and this shows that the source existence possibility around this part is high.
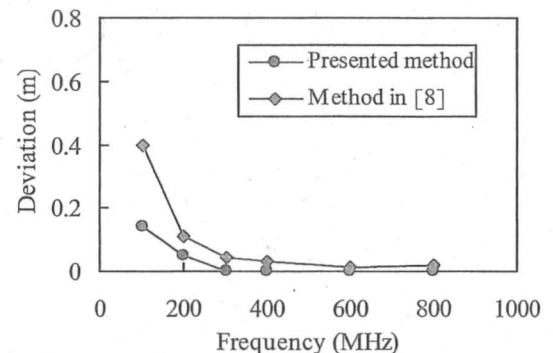

Fig. 14 Deviation between visualized and original source position for two spherical dipole antennas.
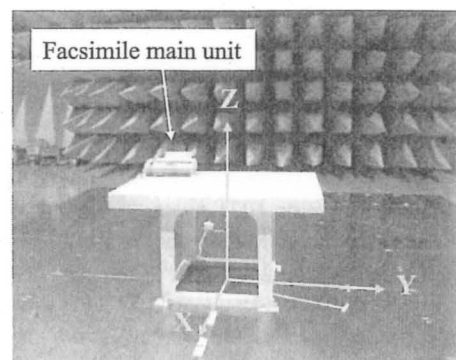

Fig. 13 Overview and signal flow for two spherical dipole antennas.

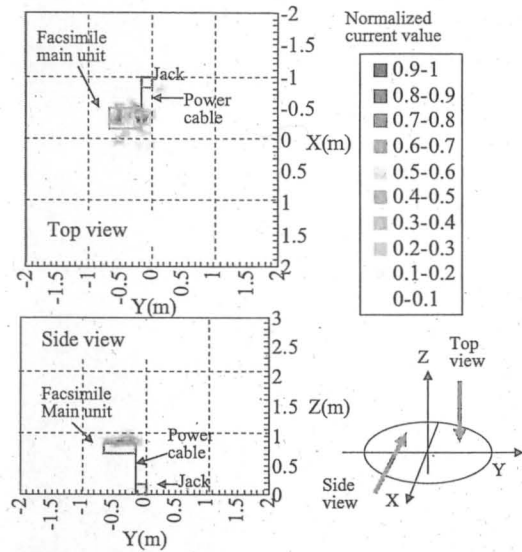Fig. 15 Overview of a facsimile as an actual EUT.

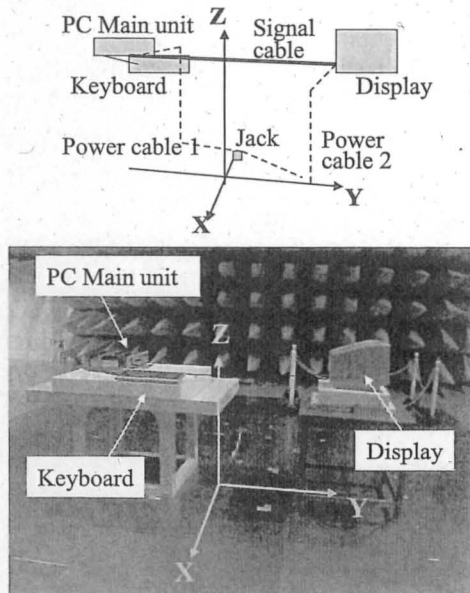**Fig. 16** Visualization result with a facsimile unit (240 MHz).

Fig. 17 Overview of a PC system as an actual EUT.

Fig. 18 Visualization result with a PC system (190 MHz).

This macroscopic visualization result agrees with the pre-measurement result; therefore the presented method could be applied to the facsimile as an actual EUT.

4.5 Results with a PC System as an Actual EUT

The facsimile described in Sect. 4.3 was a relatively simple construction for use as an EUT system. For this section, a PC system was used as a more complex EUT system. Figure 17 shows the overview of this. The system consisted of a main unit, a display, a keyboard, a power cable for the main unit, a power cable for the display and a signal cable connecting the main unit to the display. These parts were placed separately on a wide area so as to be distinguished
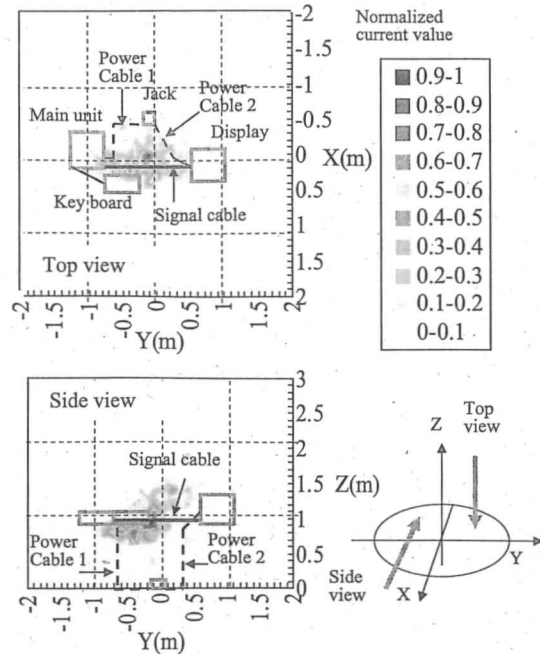
easily.

For the PC, pre-measurement was performed in the same way as was described in Sect. 4.3, and 190 MHz was chosen as the focused frequency. Next, it was attempted to identify which part dominates the radiated emission at a 3 m distance. To achieve this, the radiated emission was measured while each unit or cable was individually turned on or off, or disconnected. Furthermore, a conductive sheet was used to shield each part. From the results, it was supposed that the dominant source in the system exists on the signal cable.

The visualization result obtained by using the presented method is shown in Fig. 18, for which three sources were used according to Table 1. It can be seen that sources are visualized near the center of the signal cable (length: 120 cm) connecting the main unit with the display. Its position corresponds to the phase center of a dipole antenna when the cable is assumed to be a dipole antenna for transmitting. Sources barely exist on the main unit, the display, or the keyboard. These findings agree with the pre-measurement result; therefore the presented method could be applied to the PC system as a complex EUT.

5. Conclusion

In order to mitigate the emission radiated from electrical equipment efficiently, it is very important to establish a source visualization method. In this paper, a new method utilizing EMI facilities specified by CISPR, and which needs only cylindrically-scanned amplitude data in the far field, has been proposed.

This is based on an optimization process called the Marquardt method, in which unknown source positions and

current values are estimated. This is repeated with randomly initialized values sufficient times so as to search globally, and all estimated values are recorded. Additionally, the visualization space is three-dimensionally divided into rectangular cells. Every estimated current value in the optimization process, weighted by $Norm^2$, is sorted into the corresponding cell in which the estimated source position is located. In this case, $Norm$ is the total deviation between the estimated and measured electric field amplitudes, which demonstrates the convergence degree and the possibility of the estimated value. By displaying the sum current value of every cell, the emission source is macroscopically visualized.

Firstly, a visualization result by computer simulation for two sources was shown. Secondly, the spatial resolution was evaluated, resulting in a resolution of around 0.2 m when the cell size was 0.1 m. Subsequently, from experimental verification using a comb generator in a semi-anechoic chamber, the source was visualized with a deviation of around 0.1 m at a frequency range of 100 MHz to 800 MHz. When two spherical dipole antennas were used, the deviation was less than 0.15 m. Finally, a facsimile unit and a PC system were employed as actual EUTs. The visualization results agreed with the source locations found by another trial, and consequently the basic applicability of the presented method has been demonstrated.

Problems from the viewpoint of future works are as follows;

- Applicability to incoherent sources and a need for study on how to discriminate between coherent sources and incoherent sources.
- Applicability to high frequencies above 800 MHz
- Influence of the characteristics of a receiving antenna (directivity, size, etc.)
- Experimental verification for other EUTs, and under various conditions.
- Applicability to sources distributed along a line or in two dimensions.

References

[1] IEC/CISPR Publication 22, "Information technology equipment—Radio disturbance characteristic—Limits and methods of measurement," April 2003.
[2] M. Ohtake, Y. Matsubara, and K. Tanaka, "Development of noise visualization system for extraneous electromagnetic wave and its application to circuit design," Noise Laboratory, Noise Technical Report, vol.29, pp.1–5, 2003.
[3] R.O. Schmidt, "Multiple emitter location and signal parameter estimation," IEEE Trans. Antennas Propag., vol.AP-34, no.3, pp.276–280, March 1986.
[4] H. Kitayoshi and K. Sawaya, "Electromagnetic wave visualization for EMI using a new holography method," IEICE Trans. Commun. (Japanese Edition), vol.J80-B-II, no.3, pp.284–291, March 1997.
[5] Y. Yoshimoto, K. Taira, and K. Sawaya, "Estimation of multiple coherent source locations by using SPM method combined with signal subspace fitting technique," IEICE Trans. Commun., vol.E88-B, no.8, pp.3164–3169, Aug. 2005.

[6] T. Kato, K. Taira, and K. Sawaya, "Estimation of short range multiple coherent source location by using MUSIC algorithm," IEICE Trans. Commun., vol.E88-B, no.8, pp.3317–3320, Aug. 2005.
[7] S. Yagitani, K. Ishibana, I. Nagano, Y. Nishi, Y. Yoshimura, H. Hayakawa, and K. Tsuruta, "Location of low-frequency electromagnetic sources," IEICE Trans. Commun. (Japanese Edition), vol.J87-B, no.8, pp.1085–1093, Aug. 2004.
[8] Y. Ishida, K. Yamashita, and M. Tokuda, "Finding method of radiated emission sources with arbitrary directional current components utilizing CISPR measurement system," IEICE Trans. Commun., vol.E85-B, no.4, pp.723–731, April 2002.
[9] M. Fujimoto, N. Kikuma, and N. Inagaki, "Performance of CMA adaptive array optimized by marquardt method for suppressing multipath waves," IEICE Trans. Commun. (Japanese Edition), vol.J74-B-II, no.11, pp.599–607, Nov. 1991.
[10] H. Terashi, K. Tanaka, Y. Ishida, M. Tokuda, and N. Kuwabara, "Conditions for estimating emission sources on electric equipment using only amplitude data," IEICE Trans. Commun. (Japanese Edition), vol.J87-B, no.2, pp.226–234, Feb. 2004.
[11] C.R. Paul, Introduction to Electromagnetic Compatibility, pp.177–240, John Wiley & Sons, 1992.
[12] Y. Okubo, M. Kawabata, Y. Ishida, and N. Kuwabara, "Improvement of calculation time for estimating electromagnetic disturbance level using radiation source modeling method," IEICE Technical Report, EMCJ2005-73, Sept. 2005.

Yasuhiro Ishida received the B.S. and M.S. degrees in Electrical Engineering from Kyushu University in 1986 and 1988, respectively. He worked at Kyushu Matsushita Electric Co., Ltd. from 1988 to 1992. He joined Fukuoka Industrial Technology Center, Mechanics and Electronics Research Institute in 1992. Since then, he has been engaged in research and development in relation to EMI measurement and suppression, receiving a Ph.D. degree from Kyushu Institute of Technology in 2001. His current research interests include techniques to find radiated emission sources finding.

Masato Kawabata received the B.S. degree in Electrical Engineering and the M.S. degree in Electronics and Information Engineering from Hokkaido University in 1995 and 1997, respectively. He worked at Kawasaki Heavy Industries, Ltd. from 1997 to 2002. He joined Fukuoka Industrial Technology Center, Mechanics and Electronics Research Institute in 2002. He is presently engaged in research on EMI measurement and evaluation of an anechoic chamber.

Nobuo Kuwabara received the B.E. and M.E. degrees in Electronic Engineering from Shizuoka University in 1975 and 1977, respectively. He also holds the Ph.D. degree in Engineering from Shizuoka University, granted in 1992. Since joining NTT in 1977, he had been researching over-voltage protection of telecommunication systems, designing induction-free optical-fiber cables and electromagnetic compatibility in electro-communication systems. At present, he is a professor in the faculty of engineering, Kyushu Institute of Technology. He is a member of IEEE.